Journal of Analytical and Applied Pyrolysis 96 (2012) 153–161

Contents lists available at SciVerse ScienceDirect

Journal of Analytical and Applied Pyrolysis

journal homepage: www.elsevier.com/locate/jaap

A kinetic model for the thermal evolution of sedimentary and meteoritic organic carbon using Raman spectroscopy

David K. Muirhead, John Parnell, Colin Taylor, Stephen A. Bowden*

School of Geosciences, University of Aberdeen, Aberdeen AB24 3UE, UK

ARTICLE INFO

Article history:
Received 4 October 2011
Accepted 31 March 2012
Available online 10 April 2012

Keywords:
Raman spectroscopy
Murchison
Thermal maturity
Pyrolysis
Kinetic

ABSTRACT

Small samples of Murchison meteorite were flash pyrolysed at a range of temperatures (250–1000 degrees centigrade) for short durations (10–80 s). Raman spectroscopic analysis of the feedstock-pyrolysate revealed that with increased level of thermal alteration the R1 parameter (also known as the ID/IG and D/O ratio) increased in value. This appears to be a phenomena unique to low levels of thermal alteration and is most easily observed in homogeneous materials. An empirically derived kinetic model of the rise of the R1 parameter was obtained from the experimental data and used to successfully reproduce field measurements and experimental work from a number of short duration high temperature heating events. Results indicate that the use of this parameter and its predictor equation are limited to levels of thermal alteration less than that associated with the end of the oil window and the onset of condensate formation. It is also limited to situations where durations of heating are short. Even within these boundaries a high level of variation is observed in data from all settings which can make the parameter imprecise.

1. Introduction

The natural cycling of organic carbon in geological processes continues to be an area that receives broad scientific attention. Particularly the naturally occurring processes that conclude with the pyrolysis of organic carbon buried in sediments and rocks. Understanding and modelling the conversion of recalcitrant biological organic matter into chemically labile geological organic matter rich in aromatic carbon is important to fossil fuel chemists, petroleum geologists, Earth system scientists and astrobiologists. Examples of this include the need to assess the thermal maturity and rank of coals, which relates to coking potential and broad utility as a fuel [1,2]. Similarly petroleum source rocks, geological formations that generate petroleum under favourable conditions, are assessed during petroleum exploration programs to help select regions of the subsurface most likely to contain oil and gas [3].

For the last century a widely applied method for quantifying thermal alteration has been to measure the reflectance of a recalcitrant fossil plant detritus called vitrinite [4]. As fossil carbonaceous materials held within rocks thermally mature their chemical structure evolves via a complex series of reactions that lead to the formation and reordering of aromatic subunits into stacked layers that may eventually yield graphite [5]. During this process particulate fossil organic matter generally darkens, becomes more opaque and the reflectance of vitrinite macerals increases. This process can be numerically modelled by the Arrhenius equation where changes in the reflectivity of vitrinite macerals (fossil plant remains) can be modelled as a chemical reaction [6] or empirically as a temperature dependant process [7]. Such models are extremely powerful, particularly for petroleum exploration where they can be used to evaluate and develop geological understanding of the subsurface by backwards modelling to fit observed data.

Much recent work in analytical chemistry has developed Raman spectroscopy as a tool for evaluating the degree of thermal alteration of carbonaceous organic matter. The most widely applied method measures the intensity of two broad composite Raman bands or spectral peaks (at ~1585 cm^{-1} and ~1350 cm^{-1}) produced by the (Stokes) Raman scattering of light, typically induced by a 532 nm laser [8]. One spectral peak at ~1585 cm^{-1} is a composite of several Raman bands at ~1615, 1598 and ~1545 cm^{-1} and is initially relatively broad but narrows with increased thermal maturation as aromatic structures are formed [9]. The composite spectral peak at ~1350 cm^{-1} is predominantly influenced by a Raman band at 1345 cm^{-1} and much less so by a band at 1215 cm^{-1}, but ongoing work continues to refine the interpretation and application of the composite spectral peaks produced by these Raman bands to the fuel and particularly the natural sciences and the reader is directed to Marshall et al. [8] for a recent review.

Over the recent decades it has been common practice to obtain a number of 'Raman' or geochemical parameters by measuring these

* Corresponding author. Tel.: +44 01224 273467; fax: +44 01224272785.
E-mail address: s.a.bowden@abdn.ac.uk (S.A. Bowden).

0165-2370
http://dx.doi.org/10.1016/j.jaap.2012.03.017

spectral peaks as composite bands [2]. This includes the width and position of the composite band at ~1585 cm^{-1} often termed the G or O peak [10]. With increased thermal maturation the structural reordering of carbonaceous materials creates homogenised materials with an increased proportion of aromatic carbon; the consequence of this is that the band at 1585 cm^{-1} narrows and its spectral peak shifts to a higher position on a Raman Spectrum closer to 1615 cm^{-1} (and if graphite is formed than the peak should be closer 1598 cm^{-1}). Another parameter can be obtained by comparing the intensity of the O peak or band at ~1585 cm^{-1} to that of the D (disorder) peak or band at ~1345 cm^{-1} creating a parameter often termed the R1 ratio. This is expressed as a ratio of D/O peak areas or as a fraction in the form D/[D + O] (as may be done for fossil fuel biomarkers analysed by GC–MS). At high levels of thermal maturation and with increased structural ordering the ratio decreases, and considerable work has focused on applying the R1 parameter to metamorphic rocks [11] and ancient meteorites [12]. However, experimental work has also shown that early stage thermal alteration raises the R1 parameter (obtained from undeconvolved, composite D and O Raman Bands), both for vacuum deposited carbon films, cellulose fibres and coal char [13–15]. These observations (as with our work presented here) are for relatively homogenous materials e.g. only a single type of feedstock was considered in each case. Thus it is important to keep in mind that mixtures of different types of organic maceral would produce R1 profiles (as a function of time and temperature) that are a composite of the R1 profiles of different components [16]. Potentially this complicates observation and measurement of R1 profiles on heterogeneous natural materials.

The rise in a proxy initially intended to describe decreasing structural disorder may initially seem aberrant but the O peak, also referred to as the G peak, is a composite spectral peak comprising contributions from Raman scattering not only by graphite (unlikely to be present at low thermal maturities) but also other carbonaceous materials with aromatic sub-units. These structures occur widely in nature in higher plant biomass (e.g. lignin) and humic materials [17] and are also common constituents of the organic chondrules found in primitive and relatively unaltered meteorites such as Murchison [18,19]. It is also notable that the surface enhanced Raman spectra of solvent soluble sedimentary organic matter and humic materials (which do not contain graphite) often have very broad Raman bands at 1600–1618 cm^{-1} [20,21]. Thus there exists a range of geologically-naive carbonaceous materials that posses an aromatic character. The degradation and alteration of these compounds, and the associated decline in the relative strength of Raman Bands ~1615 cm^{-1}, is thus likely to be responsible for the initial rise of a composite R1 parameter (an R1 parameter obtained from undeconvolved, composite D and O Raman bands) during diagenesis, prior to higher levels of thermal alteration. Given the broad interest in the fate of organic matter during early diagenesis, it might be expected that changes in Raman parameters that characterise the initial stages of thermal maturation and diagenesis would have been widely studied. However, this is not the case and it is not commonly known over what range of time and temperatures and at what reaction rates this occurs – particularly with regard to the natural world.

In this work we present a kinetic model for the rise of a R1 parameter (obtained from composite, undeconcolved D and O Raman bands) during the early stages of thermal maturation (prior to thermal metamorphism) and show its rough position with respect to petroleum formation. This model is derived from experiments performed on meteoritic organic matter and then evaluated in the context of petroleum generation and the thermal evolution of sedimentary organic matter altered within the thermal aureole of an igneous dyke. This is done not only because petroleum generative processes are an economically important benchmark but also because it is a key stage in the geochemical cycling of organic carbon. It is this level of thermal alteration that coincides with organic carbon being partitioned to long term storage in the subsurface as a carbon rich thermally labile material or being altered to a volatile highly reactive compound utilised by autotrophic processes such as photosynthesis.

2. Method

All Raman Spectroscopy measurements were performed on a Renishaw inVia reflex Raman spectrometer at the University of Aberdeen, or on an identical spectrometer at the University of Glasgow. A Leica DMLM reflected light microscope was used to focus the Ar+ green laser (wavelength 514.5 nm). Laser spot size was approximately 1–2 μm and laser power between 10 and 50% (<13 mW power at the sample). At each specific point Raman spectra were acquired over 12 s with final measurements being an accumulation of 3–5 acquisitions. Care was taken to ensure that the sample did not experience any laser-induced heating, with the sample carefully analysed under the microscope (and imaged) before and after heating. For the small volume subsamples of meteoritic organic matter this equates to 25 repeat measurements per experiment, for larger volume and more naturally varied sedimentary organic matter obtained from mudstones between 50 and 75 repeat measurements were obtained.

Renishaw's WiRE 2.0 curve-fit software was used for spectral deconvolution. Smoothing and baseline extractions were performed on each sample. A cubic spline interpolation was used for baseline extraction. Each sample was deconvolved to remove a background signal at least 3 times to ensure reproducibility of data. Example spectra are shown in Fig. 1a and b. Minimal spectral processing was applied to measurement of peak areas and undeconvolved composite D and O bands were used to calculate R1 ratios (e.g. the D and O peaks were not deconvolved into smaller peaks listed in text and described in Ref. [8]).

Pyrolysis was performed on a whole rock samples using a using a CDS Instruments Pyroprobe 1000 connected to a HP 5890 gas chromatograph with a HP5972 mass spectrometer as a detector. The split/splitless injector (split ratio 1:150) and pyrolysis interface were both held at 330 °C and the helium carrier gas was flowed through the pyrolysis chamber at 1 ml per minute. Although not the main focus of this study, subsequent to each experiment, the pyrolysis products were analysed by an online GC–MS using an Agilent H5-MS1 (30 m column length, 0.250 mm ID). This method therefore permits small amounts of feedstock and pyrolysate to be compared.

Pyroprobes typically employ flash pyrolysis for analytical purposes but were employed for experimental pyrolysis in this study due to their capacity to utilise small sample volumes. This is particularly beneficial for meteoritic materials that are a limited resource. The thinly walled fused-silica pyrolysis tubes were also found to readily permit Raman spectroscopic analysis of the pyrolysis feedstock within, greatly speeding up experimental work (list of experiments provided in Table 1).

2.1. Murchison meteorite

Samples of Murchison meteorite were provided by Caroline Smith of the Natural History Museum. Additional samples of Murchison meteorite, pyrolysed by a range of pyrolysis techniques were provided by Mark Sephton of Imperial College London. The Murchison meteorite is a CM2 carbonaceous chondrite that fell in Australia in 1969 and has subsequently provided much of the current understanding of meteoritic organic matter. High molecular weight macromolecular insoluble organic matter (the fraction

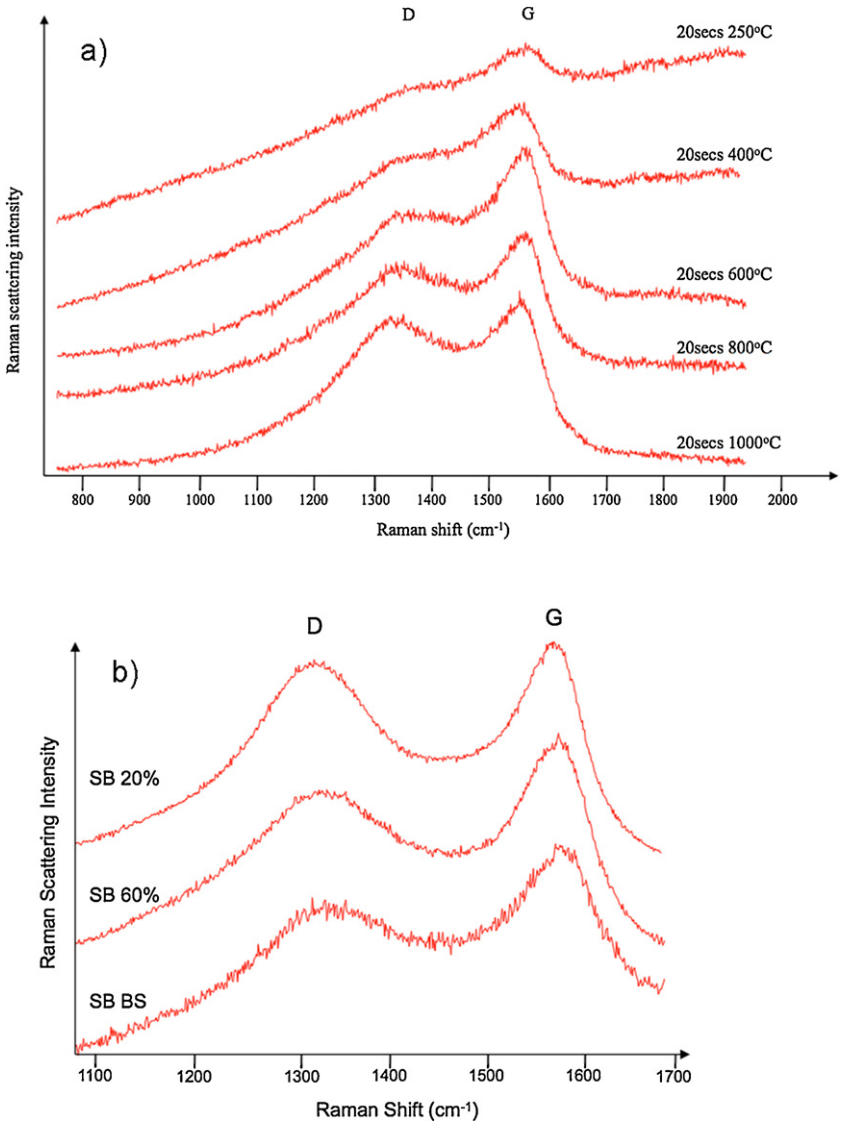

Fig. 1. (a) Raman spectra for samples of Murchison meteorite experimental pyrolysed during this study. (b) Obtained for samples of mudrock thermally matured within the aureole of an igneous intrusion: SB 20% and SB 60% are samples obtained at proximities to the dyke corresponding to 20 and 60% of the dykes total thickness; SB BS is a background sample obtained outside of the thermal aureole of the dyke.

of organic carbon most amenable to characterisation by Raman microspectroscopy) comprises a majority of Murchison's organic material, at least 70% of the meteorite's total organic content [22]. The meteorite has been extensively analysed and thus there is a considerable legacy of data; these results generally suggest that the solvent insoluble organic matter present in Murchison primarily comprises aromatic sub-units and has been compared to Type III organic matter [22].

Table 1

Duration (s)	Temperature (°C)		
	250	600	1000
5	nd	d	d
10	d	d	d
20	d	d	d
40	d	d	d
80	nd	d	nd

d = data; nd = no data.

2.2. Samples metamorphosed by dyke

Samples of mudrock rich in organic carbon and thermally altered to varying levels were obtained from the metamorphic aureole of an igneous dyke. The dyke used for this purpose is a Palaeogene-aged dolerite dyke that has intruded discordantly into Jurassic Oxford Clay shales located on the Isle of Sky, Scotland. The dyke is 4 m thick and samples were collected at increments of 40 cm from the intrusion contact out to a distance of 100 percent of the dyke thickness (%dt), at distances greater than this sampling was less frequent. Samples were collected from at least 20 cm beneath the outcrop surface to avoid the effects of weathering.

3. Results

3.1. Artificial pyrolysis of Murchison meteorite

For most of the heating durations and temperatures used in this study (5–80 s and 250–1000 °C) the R1 parameter increased – except for heating at 250 °C for the shortest durations where little change was observed. The greatest increases in the R1 parameter

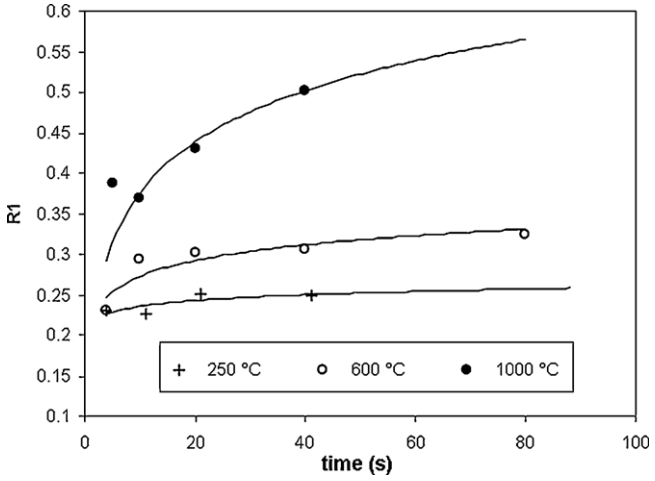

Fig. 2. Average value of R1 Raman-parameter for variably pyrolysed samples of Murchison Meteorite feedstock. $n = 275$ with 3–5 spots analysed per data point. Tie-lines for data are shown in Fig. 5. $n = 275$ with 3–5 spots analysed per data point.

and the greatest rates of change were observed for the heating experiments performed at 1000 °C (Fig. 2). Also shown for comparative purposes are data for the methyl naphthalene ratio (MNR) thermal maturity parameter measured on pyrolysis products (Fig. 3). Within naturally occurring meteoritic and sedimentary organic matter methylnaphthalenes predominantly comprise a mixture of two isomers; 1- or 2-methylnapthalene in which the methyl groups are respectively in the α and β positions [5]. With increased heating and thermal maturation the proportion of the 2-methylnapthalene isomer increases. The change in the proportion of these two isomers can be expressed as a ratio of the abundance of the two isomers, which rises in value with increased thermal maturation. Thus the higher values of this ratio observed for experiments performed at the hottest temperatures and longest heating durations help demonstrate that the meteoritic organic matter was thermally altered during experiments. In comparison to the MNR parameter the R1 parameter can be seen to change proportionally more for heating at higher temperatures.

Thus it is clear for all pyrolysates (both altered feedstock and evolved products) that increased thermal alteration resulted from heating at higher temperatures and/or heating for longer durations. For both parameters, (Figs. 2 and 3) as noted by previous workers [3,5–7], thermal alteration depends more heavily on temperature

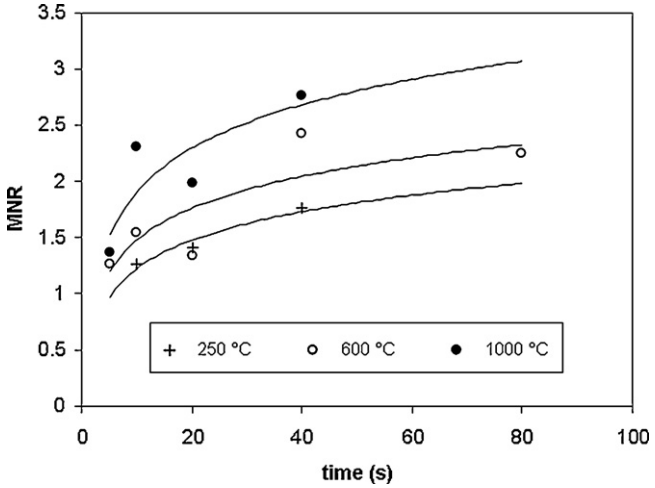

Fig. 3. Methyl naphthalene ratio for variably pyrolysed samples of Murchison meteorite pyrolysate.

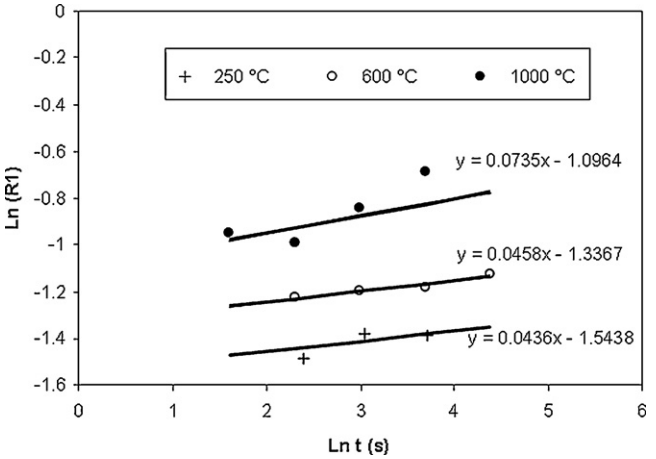

Fig. 4. Data used to determine reaction rate for the thermal evolution of the R1 parameter. Note reaction rate, given by slope of graph, increases with temperature.

then on time and does not appear first order, thus thermal evolution of the R1 parameter is better described by the power law:

$$\mathrm{R1} = kt^n \tag{1}$$

where R1 = area of composite D band denominated by the composite O band (e.g. the ratio of undeconvolved D and O Raman spectral peaks); k is the rate constant, t the duration of heating and n is a constant specific to a given temperature.

Following the example of Huang [7] for modelling the thermal evolution of vitrinite reflectance, logarithms can be taken to rewrite Eq. (1) as:

$$\ln \mathrm{R1} = \ln k + n \cdot \ln t \tag{2}$$

The functions yielded plot on straight lines with n as the slope and $\ln k$ as an intercept. Straight lines fitted to experimental data are shown in Fig. 4 and from this it can be seen that reaction rate (intercept on $\ln k$ axis) increases with temperature, however the slope n also appears to be a function of temperature. Previous empirical models of reaction rates for vitrinite reflectance have found that for the temperatures used this was not significant [7]. This variation is significant for the R1 data shown in Fig. 4, and must be considered.

The reaction rate is given by the Arrhenius equation $k = A \cdot e^{-m \cdot T}$ where A and m can be found graphically by use of an Arrhenius plot (see Supplementary Fig. S1). The values returned by this method are $A = 0.441557\ s^{-n}$ and $m = 402$.

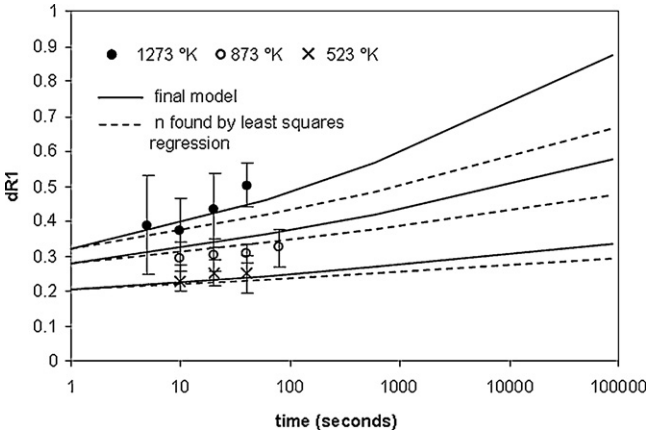

Fig. 5. Application of Eq. (5) to backmodel experimental data. Dashed line illustrates model produced by b and c from Eq. (5) being found by least squares regression. Solid line is where b and c are obtained by iteratively changing parameters to fit high temperature experiments.

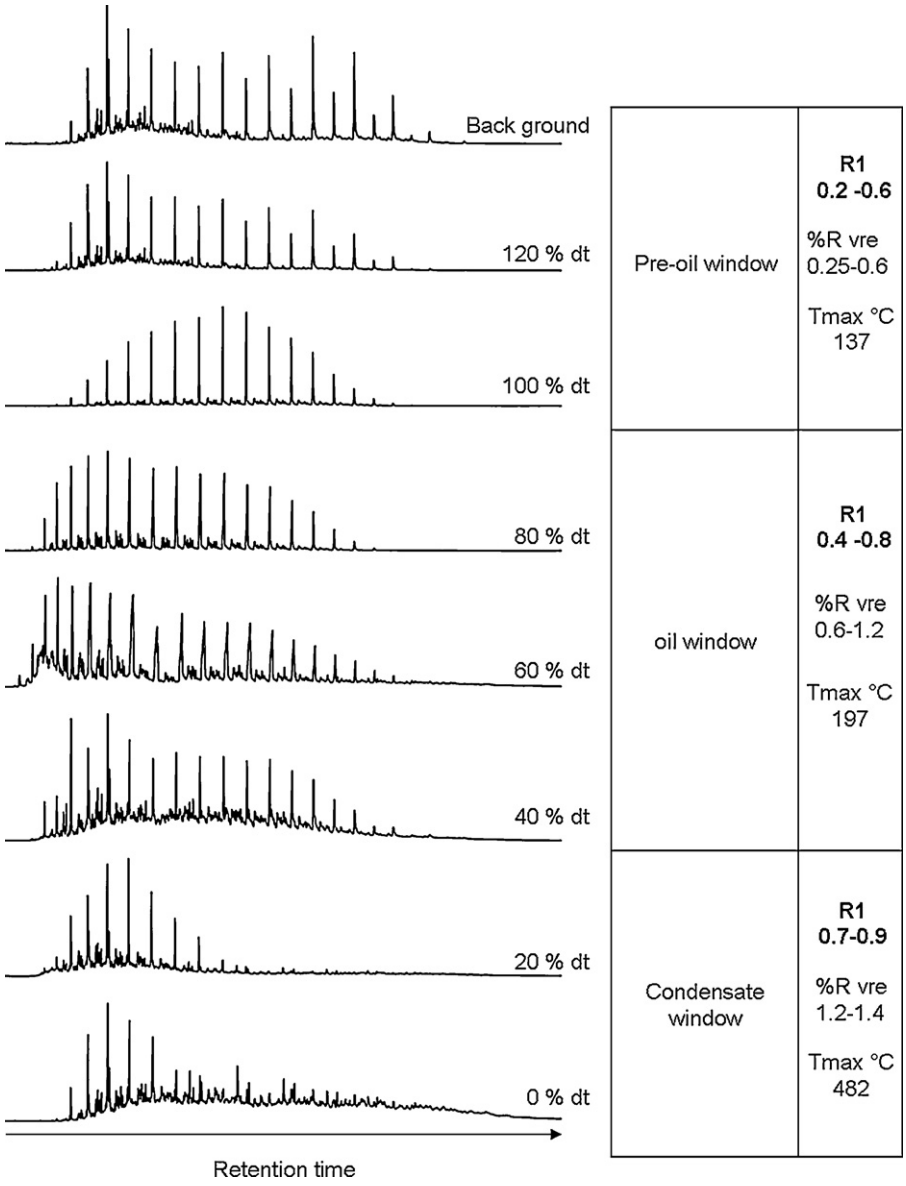

Fig. 6. 85 *m*/*z* ion chromatograms for solvent extractable organic matter from Staffin Bay fieldsite. GC-envelope and the relative prominence of certain *n*-alkane homologues illustrates key stages of petroleum formation for given distances from igneous intrusion (expressed percentage dyke thickness – %dt). Data permits the R1 parameter to be benchmarked against stages of oil generation. Comparisons are also made to maximum pyrolysis temperature (Tmax) and percentage vitrinite equivalence (%R vre) deduced from hopane and other biomarker parameters (data not shown).

Rewriting Eq. (2) to incorporate the Arrhenius equation it becomes:

$$\mathrm{R1} = A \cdot \exp^{-m/T} \cdot t^{n} \tag{3}$$

However, the above equation is unsatisfactory, as it can be seen that n is also a function of temperature (see Supplementary Fig. S2). Taking $n = T \cdot b + c$ Eq. (3) becomes:

$$\mathrm{R1} = A \cdot \exp^{-m/T} \cdot t^{T \cdot b + c} \tag{4}$$

where b and c are the slope and intercept of a straight line describing the relationship between temperature and n. These values were originally obtained by a least squares regression of experimental data, but were iteratively modified to produce R1 values that best fitted the values of R1 obtained from highest temperature and longest duration heating experiments. The final values used for the data shown in Fig. 5 (and Fig. 9 described later) are $b = 6.04\mathrm{E}{-5}$ and $c = 0.011304$ (Fig. 5 also illustrates the application of this empirical model without this adjustment).

Thus the final equation used to predict early changes in the R1 parameter as a function of temperature and heating duration are:

$$\mathrm{R1} = B + 0.441557 \exp\left(-\frac{402}{T}\right) \cdot t^{(T \cdot 6.04\mathrm{E}-5+0.011304)} \tag{5}$$

where t is the duration of heating in s, T is the temperature in degrees Kelvin and B the initial value of R1 prior to t.

3.2. Application to field site

To further investigate the model it was applied to samples of mudrock that have been heated in the thermal aureole of an igneous dyke. The dyke concerned is a 4 m thick dolerite dyke that intrudes into an organic carbon rich interval of the Oxford Clay on the Isle of Skye. The thermal aureoles around such dykes are relatively short lived and form when molten rock intrudes into sediments and sedimentary rocks [23]. Assuming heat is transferred by conduction then temperatures are initially high adjacent to the intruding body

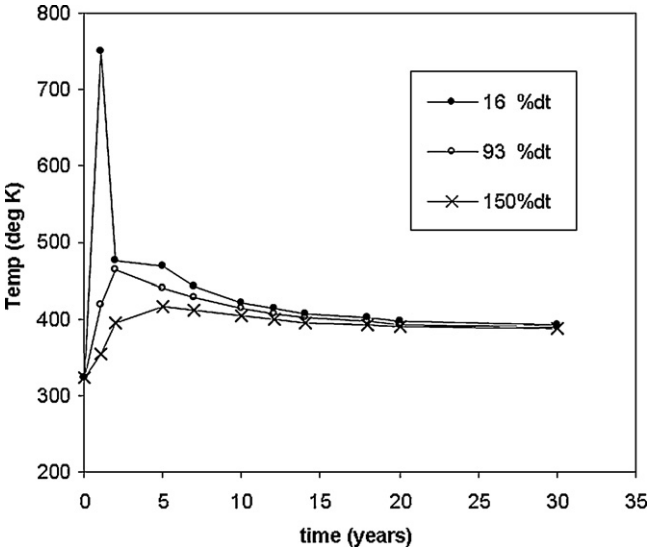

Fig. 7. Cooling curves calculated by thermic for the mudrock adjacent to the dyke in Staffin Bay.

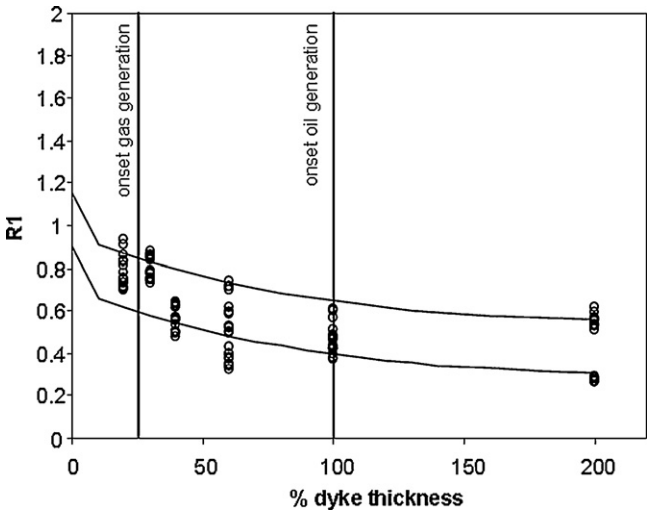

Fig. 8. Comparison of R1 values observed for mudrock within the thermal aureole of the basaltic dyke (open circle) against predictions made using Eq. (5) and the heating profiles in Fig. 7. Two models – solid and dashed lines – are used because two background values are indicated for the initial R1 value.

but decrease rapidly with time and more generally with distance expressed as a percentage of the intruding dykes thickness. The consequence of this is that further from the intrusion temperature rises slowly as heat from the cooling igneous body must be conducted over a greater distance. The effects of these different thermal regimes can be seen in differing levels of thermal alteration experienced by organic matter (Fig. 6). GC–MS ion chromatograms obtained for bitumen at different distances from the dyke evidence different levels of petroleum generation. Biologically inherited carbon number preferences for odd carbon numbered *n*-alkanes are not seen at proximities closer than 120% dyke thickness, a GC-envelope consistent with the average carbon number of oil is seen at 80% dyke thickness (marking the onset of petroleum formation) and GC-envelopes for samples closer than 20% dyke thickness evidence significant decreases in carbon number typical of the onset of hydrocarbon cracking and gas generation (Fig. 6).

Being able to recreate the effect a thermal aureole around an igneous intrusion is often employed as a test of a thermal maturity parameter [24,25]. The temperature profiles shown in Fig. 7 were obtained using Thermic, a computer program that solves the heat equation using the finite element method [26]. The model used for this study comprises a coarse grid with localised refinement adjacent to and above the dyke to stratigraphically resolve the mudstone horizon. The R1 parameters obtained using Eq. (5) are shown in Fig. 8. Two initial R1 values (*B* parameter in Eq. (5)) were used to represent the two R1 populations evidenced in background data and generally show a good fit to the model. The same model was applied to pyrolysis data generated via the approach used to artificially mature samples of Murchison meteorite, and here also a close fit is observed (Fig. 9).

4. Reliability, stability and utility

Before evaluating Eq. (5) as a predictor for time (heating duration) and temperature combinations that yield a given R1 value, it is important to briefly note the complications that arise in the measurement of Raman parameters.

Many of the complications relating to the application of Raman spectroscopy to geochemistry arise from the mathematical processing of Raman spectra to obtain the area of a given spectral feature or peak. Aside from decisions made by an operator that may effect precision or technical considerations that effect overall accuracy [26,27], it has been shown that deconvolving synthetically constructed Raman spectra of carbonaceous materials from noise and background signals is inherently difficult – peaks may both broaden and maxima shift position [28]. Furthermore, dispersion can arise due to natural variability in the chemical composition of heterogeneous materials (e.g. heteroatom content), the wavelength of excitation and the crystallographic orientation of certain materials with respect to the direction of polarisation of the light source [9]. In the worst case scenario all of these factors may give rise to the spread of data seen in Figs. 5, 8 and 9. Thus there are a number of factors, aside from duration of heating and temperature, that might cause variation in Raman-parameters intended to proxy thermal maturation. To this list it is also necessary to add naturally occurring factors such as the variability of fossil organic matter (e.g. different biomaterials from higher plants and phytoplankton) and the presence of derived phytoclasts (organic matter that has previously been buried, then thermally altered before being eroded,

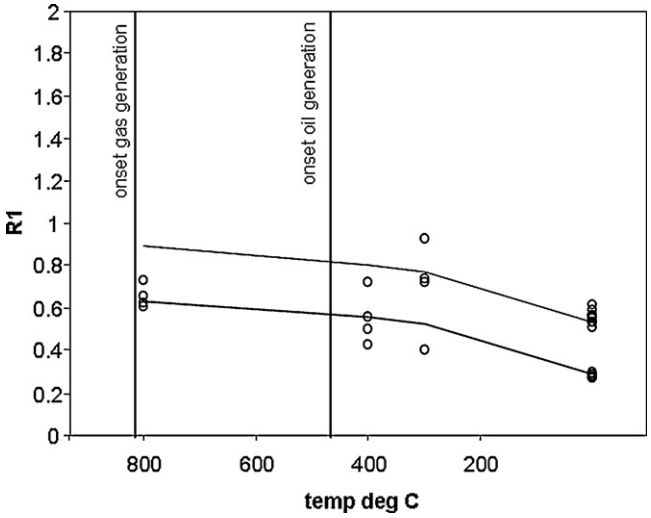

Fig. 9. Comparison of R1 values observed for kerogen subjected to the pyrolysis method used to obtain data in Fig. 2 (open circle) with predictions made using Eq. (5) and the heating profiles in Fig. 7. Pyrolysis was performed at 20 s for the time indicted. Two models – solid and dashed lines – are used because two background values are indicated for the initial R1 value.

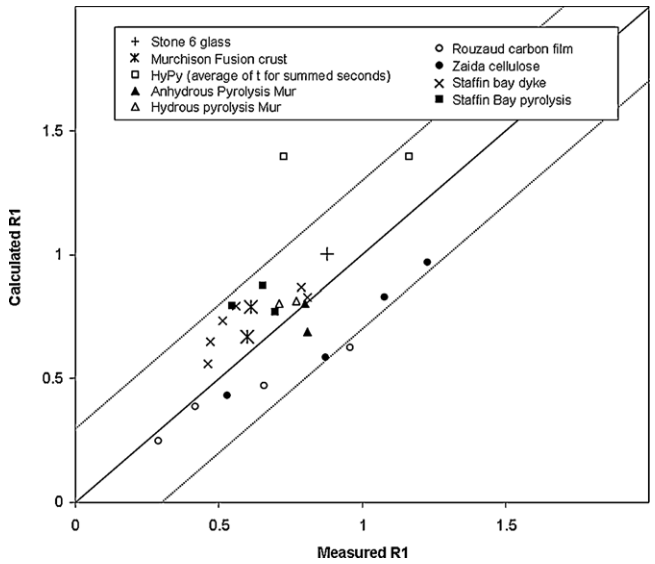

Fig. 10. Eq. (5) applied to predicting R1 values for a variety of experimental and geological cases. Solid line corresponds to 1:1 fit and dashed lines to the greatest variation typical of R1 values measured in natural samples.

exhumed, redeposited and buried again). Additionally, differences in the pyrolysis process that occur in both nature and experimentally (e.g. system pressure, presence of naturally occurring catalysts and the openness of the pyrolysis system) may interact with all the aforementioned factors creating the potential for a number of different pathways for the thermal evolution of the R1 parameter. As much as is possible these factors will be considered in the following sections.

4.1. Variability due to precursor organic material/feedstock

The Raman spectra of geological carbonaceous materials only provides information on their chemical structure and this information itself is not sufficient evidence of biogenicity [8]; it has been demonstrated that the Raman spectra of combustion products and products of geological thermal metamorphism may yield similar Raman spectra [29]. Despite this it might be hypothesised that at low levels of thermal alteration the different chemical structure of precursor biological and abiological materials would yield different thermal evolution pathways for the R1 parameter. Fig. 10 illustrates the application of Eq. (5) to predict the results of thermally maturing cellulose fibres and vacuum deposited carbon films [13,14]. From this and the data presented in Fig. 10 it can seem that the thermal maturation of both biological and non-biological feedstock yields materials with R1 values that may be predicted by the same equation. Thus, within the natural variability typically observed for the R1 parameter, Eq. (5) is able to adequately predict thermal maturation pathways for both biological and non-biological organic matter. However, this likely reflects the variability inherent in measuring the R1 parameter rather than common reaction kinetics for chemically heterogeneous materials.

4.2. Variability due to pyrolysis conditions

Different pyrolysis environments, including system pressure and the existence of an open or closed system and the presence or absence of water and the presence or absence of naturally occurring geological catalysts can all produce different degrees of thermal maturation in the same feedstock, even for identical heating durations and temperatures [30–32]. A considerable legacy of pyrolysis data exists for the Murchison meteorite [18,19] and the samples plotted in Fig. 10 include data for a variety of pyrolysis conditions including anhydrous and hydrous (water phase present) pyrolysis performed within pressure vessels (closed system) and also fixed bed pyrolysis performed in the presence of excess hydrogen (hydropyrolysis – an open pyrolysis system). Excepting hydropyrolysis data, where one sample was less thermally altered than predicted, R1 values for all thermally altered samples were predicted within the bounds of naturally encountered variation. Therefore, while the aforementioned variables in pyrolysis conditions clearly have profound effects on the thermal evolution of sedimentary organic matter and the products that are generated – the effects of these factors on the R1 Raman parameter are less than the natural variability of measured R1 values.

The high temperature short duration pyrolysis conditions employed in this study closely resemble those proposed for the genesis of fusions crusts (the melted layer of rock formed on the exterior of meteorites) during atmospheric entry [33]. The heating curves generated by Kimua et al. [33] for the fusion crust and melt-phases of Yamoto 75267 were used to predict R1 values for carbonaceous organic matter found in the Murchison meteorite fusion crust and 5 mm beneath it (the thermal histories used where 1400 °C for 3 s for carbonaceous materials within the fusion crust and 400 °C for 10 s for carbonaceous materials 5 mm beneath the crust). Similarly a R1 value was also calculated for the organic matter within the fusion crust generated by exposing a sample of mudrock to atmospheric entry (1840 °C for 150 s) on the exterior of a Russian-Photon spacecraft during the ESA Stone 6 mission [34]. These predictions (Fig. 10) slightly exceed measured values, but place the samples in the correct order of thermal alteration, e.g. the exterior fusion crust is more altered than the samples beneath it thus the effects of “short-hot” heating were differentiated from “longer-cooler” heating.

4.3. Reliability

A key limit of the approach taken here to model thermal evolution of the R1 parameter, is that the model is empirically fitted to observations. The consequence of this is that little can be deduced about the nature of the chemical reactions and changes in molecular structure responsible for brining about changes in the R1 Raman parameter. A similar distinction applies to models of vitrinite reflectance. There are models of the thermal evolution of the vitrinite reflectance parameter that are based on rate constants for chemical reactions that generate methane, carbon dioxide and water and take account of the different activation energies required for these reactions [6]. Thus the effect of the different reaction rates for these processes can be considered and the thermal alteration pathways of different organic matter compositions can then be explored e.g. oil and gas prone kerogen for example. In contrast, models empirically fitted to data (such as Huang [7] and this study) do not permit this level of investigative analysis. From an applied point of view this may not be of consequence for a number of reasons. Foremost is that the assumptions made to permit backwards modelling for many geological applications (e.g. thermal alteration during burial of organic matter or during a metamorphic event) and the variability observed in data used to truth these models are very broad. Additionally models based on empirical observations are computationally light [7] and easily adjusted or calibrated to a given situation.

4.4. Stability

Relative to the thermal alteration of sedimentary organic matter to generate petroleum the geological metamorphism of inorganic minerals is usually characterised by heating durations many orders of magnitude longer and temperatures that are twice to ten times

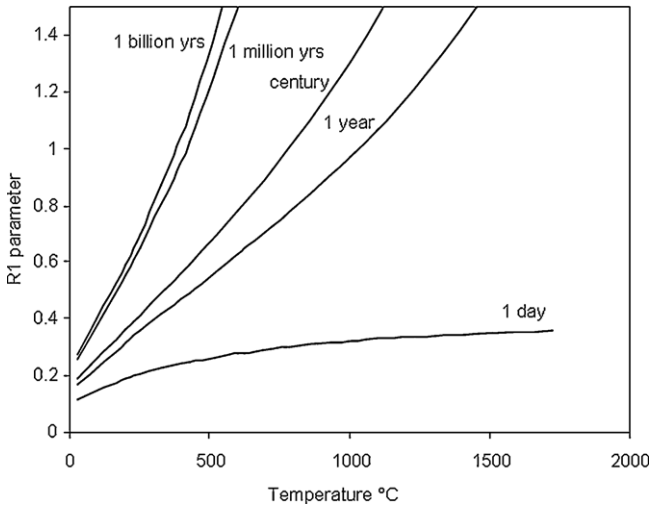

Fig. 11. Predictions of R1 values for different time temperature domains. It is notable that for durations of heating only relevant to geological situations that time is not particularly important. Additionally at these time scales the parameter reaches its maximum value (prior to the parameter inverting/falling) at temperatures associated low grades of metamorphism (Prehnite-Pumpellyite grade).

as high. Within this time and temperature domain the R1 parameter decreases with increasing thermal alteration [10], as opposed to increasing as is observed at lower levels of thermal alteration. The highest values reported for the R1 parameter measured in naturally occurring organic materials are about 1.5 for of coal [10] and 1.6 the Allende meteorite (a carbonaceous chondrite that has experienced greater thermal alteration than the Murchison meteorite) [12]. From Fig. 11 it is clear that heating durations of 1–10 millions of years at temperatures associated with Prehnite-Pumpellyite grade metamorphism (>300 °C where chlorite is often the distinctive member of a metamorphic mineral assemblage) maximum values reported for the R1 parameter are approached or exceeded. It is also clear that heating duration is a less important factor when geological time scales are considered (1 million to 1 billion years). Beyond these temperatures and heating durations Eq. (5) cannot predict values of the R1 parameter, although other predictor equations based on parameters derived from Raman spectroscopy are known [12]. This domain of time and temperature corresponds to the lowest grades of metamorphism reported by Wopenka and Pastiris [10] subsequent to which the R1 parameter inverts and decreases in value with increased thermal metamorphism.

4.5. Utility

While Eq. (5) predicted R1 values within the range of natural variability for most cases, it is important to note the variability of R1 values for a given sample evidenced in Figs. 8 and 9 is considerable (±0.25). Based on the characteristics of the petroleum observed within the vicinity of the Staffin Bay dyke R1 values of 0.6–0.9 (average 0.85) are associated with the early gas window and 0.3–0.6 the oil window. Thus demarcation of the onset of key changes in the nature of petroleum generation by the R1 parameter utilises thresholds near to naturally observed variation! However, this is not a flaw unique to this geochemical proxy of thermal alteration, and many parameters such as the temperature of maximum pyrolysis yield, parameters based on the opacity of palynomorphs such as the spore colouration index and even vitrinite reflectance can all evidence similar scatter [35] under different circumstances.

5. Conclusions

An empirical rate equation has been demonstrated for the thermal evolution of the R1 Raman parameter during early to late diagenesis. The predictor equation was derived from extraterrestrial organic matter and is especially suited to predicting high temperature short duration heating events. Despite this it can be shown to be relevant to durations of heating associated with contact metamorphism and make reasonable predictions for longer term geological heating up until the onset of levels of thermal alteration commensurate with geological metamorphism.

Acknowledgements

We thank Caroline Smith and Mark Sephton for provision of samples of Murchison meteorite and Peter Chung for access to Raman Spectroscopy facilities at the University of Glasgow. DKM gratefully acknowledges receipt of an EPSRC doctoral training grant.

Appendix A. Supplementary data

Supplementary data associated with this article can be found, in the online version, at doi:10.1016/j.jaap.2012.03.017.

References

[1] L. Thomas, Coal Geology, John Wiley & Sons Ltd, Chichester, England, 2002.
[2] S. Potgieter-Vermaak, N. Maledi, N. Wagner, J.H.P. Van Heerden, R. Van Grieken, J.H. Potgieter, Raman spectroscopy for the analysis of coal: a review, Journal of Raman Spectroscopy 42 (2) (2011) 123–129.
[3] J.M. Hunt, Petroleum Geochemistry and Geology, W.H. Freeman, New York, USA, 2005.
[4] B. Durand, Elemental analysis of kerogen, in: B. Durand (Ed.), Kerogen a – Insoluble Organic Matter from Sedimentary Rocks, Editions Technip, Paris, 1980, pp. 13–34.
[5] S.D. Killops, V.J. Killops, Introduction to Organic Geochemistry, Blackwell Science Ltd., Blackwell Publishing Company, USA, 2005.
[6] A.K. Burnham, J.J. Sweeny, A chemical kinetic model of vitrinite reflectance and maturation, Geochimica et Cosmochimica Acta 53 (1989) 649–2657.
[7] W. Huang, Experimental study of vitrinite maturation: effects of temperature, time, pressure, water and hydrogen index, Organic Geochemistry 24 (1996) 233–241.
[8] C.P. Marshall, H.G.M. Edwards, J. Jehlicka, Understanding the application of Raman spectroscopy to the detection of traces of life, Astrobiology 10 (2) (2010) 229–243.
[9] A.C. Ferrari, J. Robertson, Interpretation of Raman spectra of disordered and amorphous carbon, Physical Review B – Condensed Matter and Materials Physics 61 (20) (2001) 14095–14107.
[10] B. Wopenka, J.D. Pasteris, Structural characterization of kerogens to granulite-facies graphite: applicability of Raman microprobe spectroscopy, American Mineralogist 78 (5–6) (1993) 533–557.
[11] T.-F Yui, E. Huang, J. Xu, Raman spectrum of carbonaceous material: a possible metamorphic grade indicator for low-grade metamorphic rocks, Journal of Metamorphic Geology 14 (2) (1996) 115–124.
[12] H. Busemann, C.M.O'D. Alexander, L.R. Nittler, Characterization of insoluble organic matter in primitive meteorites by microRaman spectroscopy, Meteoritics and Planetary Science 42 (7–8) (2007) 1387–1416.
[13] J.N. Rouzaud, A. Oberlin, C. Beny-Bassez, Carbon films: structure and microtexture (optical and electron microscopy, Raman spectroscopy), Thin Solid Films 105 (1) (1983) 75–96.
[14] A. Zaida, E. Bar-Ziv, L.R. Radovic, Y.-J. Lee, Further development of Raman Microprobe spectroscopy for characterization of char reactivity, Proceedings of the Combustion Institute 31 (II) (2007) 1881–1887.
[15] C. Sheng, Char structure characterised by Raman spectroscopy and its correlations with combustion reactivity, Fuel 86 (15) (2007) 2316–2324.
[16] V.P. Chabalala, N. Wagner, S. Potgieter-Vermaak, Investigation into the evolution of char structure using Raman spectroscopy in conjunction with coal petrography; Part 1, Fuel Processing Technology 92 (4) (2011) 750–756.
[17] P.G. Hatcher, D.J. Clifford, The organic geochemistry of coal: from plant materials to coal, Organic Geochemistry 27 (5–6) (1997) 251–274.
[18] M.A. Sephton, C.T. Pillinger, I/Gilmour, small-scale hydrous pyrolysis of macromolecular material in meteorites, Planetary and Space Science 47 (1–2) (1998) 181–187.
[19] M.A. Sephton, G.D. Love, J.S. Watson, A.B. Verchovsky, I.P. Wright, C.E. Snape, I. Gilmour, Hydropyrolysis of insoluble carbonaceous matter in the Murchison meteorite: new insights into its macromolecular structure, Geochimica et Cosmochimica Acta 68 (6) (2004) 1385–1393.

[20] E. Vogel, R. Geßner, M.H.B. Hayes, W. Kiefer, Characterisation of humic acid by means of SERS, Journal of Molecular Structure 482–483 (1999) 195–199.
[21] S.A. Bowden, R. Wilson, J.M. Cooper, J. Parnell, The use of surface-enhanced Raman scattering for detecting molecular evidence of life in rocks, sediments, and sedimentary deposits, Astrobiology 10 (6) (2010) 629–641.
[22] M.A. Sephton, Organic compounds in carbonaceous meteorites, Natural Product Reports 19 (3) (2002) 292–311.
[23] T.S. Lovering, Theory of heat conduction applied to geological problems, Geological Society of America Bulletin 46 (1935) 69–94.
[24] Bostick, Paleotemperatures based on vitrinite reflectance of shales and limestones in igneous dike aureoles in the Upper Cretaceous Pierre Shale, Walsenburg, Colorado, in: N.H. Bostick, M.J. Pawlewicz (Eds.), Hydrocarbon Source Rocks of the Greater Rocky Mountain Region, Rocky Mountain Association of Geologists, Denver, CO, U.S.A, 1984, pp. 387–392.
[25] J.J. Sweeney, A.K. Burnham, Evaluation of a simple model of vitrinite reflectance based on chemical kinetics, American Association of Petroleum Geologists Bulletin 74 (10) (1990) 1559–1570.
[26] A. Bonneville, P. Capolsini, THERMIC: a 2-D finite-element tool to solve conductive and advective heat transfer problems in Earth Sciences, Computers and Geosciences 25 (10) (1999) 1137–1148.
[27] E. Smith, G. Dent, Modern Raman Spectroscopy, John Wiley & Sons, Chichester, England, 2005.
[28] A. Rotundi, G.A. Baratta, J. Borg, J.R. Brucato, H. Busemann, L. Colangeli, L. D'Hendecourt, Z. Djouadi, G. Ferrini, I.A. Franchi, M. Fries, F. Grossemy, L.P. Keller, V. Mennella, K. Nakamura, L.R. Nittler, M.E. Palumbo, S.A. Sandford, A. Steele, B. Wopenka, Combined micro-Raman, micro-infrared, and field emission scanning electron microscope analyses of comet 81P/Wild 2 particles collected by Stardust, Meteoritics and Planetary Science 43 (1–2) (2008) 367–397.
[29] J.D. Pasteris, B. Wopenka, Necessary, but not sufficient: Raman identification of disordered carbon as a signature of ancient life, Astrobiology 3 (4) (2003) 727–738.
[30] M.D. Lewan, Experiments on the role of water in petroleum formation, Geochimica et Cosmochimica Acta 61 (17) (1997) 3691–3723.
[31] M.D. Lewan, Evaluation of petroleum generation by hydrous pyrolysis experimentation, Philosophical Transactions of the Royal Society of London 315 (1997) 123–134.
[32] S.-T. Lu, I.R. Kaplan, Hydrocarbon-generating potential of humic coals from dry pyrolysis, American Association of Petroleum Geologists Bulletin 74 (2) (1990) 163–173.
[33] M. Kimura, M. Chen, Y. Yoshida, A. El Gorsey, E. Ohtani, Back-transformation of high pressure phases in a shock melt vein of an H-chonrite during atmospheric passage: implications for the survival of high pressure phases after decompression, Earth and Planetary Science Letters 217 (2003) 141–150.
[34] Parnell, S.A. Bowden, D. Muirhead, N. Blamey, F. Westall, R. Demets, S. Verchovsky, F. Brandstätter, A. Brack, Preservation of organic matter in the STONE 6 artificial meteorite experiment, Icarus 212 (1) (2011) 390–402.
[35] B.P. Tissot, D.H. Welte, Petroleum Formation and Occurrence, 1984.